Supplementary Materials for

Deep-Nanohole-Clad Waveguides with Depth-to-Diameter Ratio up to 50,000 in Single Crystals via Femtosecond Laser Writing

Bowen Fan[1,†], Yuying Wang[1,†], Jiacheng Hu[1], Xuhu Han[1], Lijing Zhong[2,*], and Jianrong Qiu[1,*]

[1] State Key Laboratory of Extreme Photonics and Instrumentation, College of Optical Science and Engineering, Zhejiang University, Hangzhou 310027, China.

[2] Institute of Light+X Science and Technology, College of Information Science and Engineering, Ningbo University, Ningbo 315211, China.

*zhonglijing@nbu.edu.cn

*qjr@zju.edu.cn

†These authors contributed equally to this work and should be considered co-first authors.

1.Physical Mechanism of Spherical Aberration (SA) Enhanced Focusing

In standard femtosecond laser processing using high-numerical-aperture (NA) objectives, the focal volume is governed by the diffraction limit. While high-NA objectives achieve tight lateral confinement (radius w_0), they inherently result in a significantly shortened depth of focus (Rayleigh length, z_R), This creates a fundamental trade-off: tight focusing leads to a short interaction length, making it physically impossible to modify high-aspect-ratio volumes in a single pulse. Furthermore, the perfect constructive interference at the focus results in an extremely high peak intensity , which often exceeds the threshold for micro-explosion, leading to uncontrollable cavitation and void formation[1].

To overcome these limitations, we intentionally introduce a defined amount of spherical aberration by inserting a thick YAG plate (thickness d, refractive index n_{YAG}) into the optical path. This plate introduces a nonlinear phase delay across the wavefront. The phase shift $\Phi(\theta)$ accumulated by a ray entering at angle θ can be expressed as:

$$\Phi(\theta) = kd(n_{YAG}\cos\theta' - \cos\theta),$$

where k is the wavenumber and θ' is the refracted angle inside the plate (derived from Snell's law). Due to this phase modulation, paraxial rays and marginal rays focus at different axial positions. This longitudinal spherical aberration distributes the optical energy along the propagation axis, transforming the focal point into an elongated, "needle-like" focal line.

The redistribution of energy along the extended focal line (length >100 μm) significantly alters the laser-matter interaction dynamics. By stretching the focal energy axially, the local peak intensity is effectively attenuated compared to the diffraction-limited case ($I_{SA}<I_{Gauss}$). This enables a distinct "gentle" modification regime: The extended "needle" ensures uniform energy deposition along the depth, facilitating the formation of continuous, smooth structural changes (amorphization) rather than discrete voids. This mechanism is the key enabler for fabricating void-free, high-depth-to-diameter ratio nanoholes.

2.Mechanism of Depth-Insensitive Nanohole Formation: Spherical Aberration and Threshold Effect

In our experimental configuration, a 3-mm-thick window is placed on top of the sample. On the one hand, this window significantly enhances spherical aberration, leading to pronounced axial elongation of the focal field inside the material. On the other hand, the depth-dependent variation of the focal field within the sample is relatively un-remarkable, resulting in consistent nanohole lengths across different depths. Both theoretical simulations and experimental results demonstrate that the effective modification length is insensitive to processing depth under this aberration-engineered focusing condition.

We employed numerical simulations to calculate the three-dimensional focal intensity distributions inside sapphire at different fabrication depths2 (Fig. S2.), taking into account refraction and spherical aberration induced by a 3-mm-thick YAG cover plate. The simulations show the axial Full Width at Half Maximum (FWHM) varies from 202.3 μm to 268.3 μm, while the transverse main lobe width remains stable between 46 and 54 μm. Revealing that the focal field evolution is insensitive to depth variations. Crucially, this stability is further reinforced by the material modification threshold effect. Although the optical focal line theoretically elongates with increasing depth due to accumulated spherical aberration, the peak intensity simultaneously decreases as the energy spreads out. Consequently, only the central portion of the focal line, where the intensity remains above the modification threshold—effectively contributes to the material removal. As a result, the actual length of the fabricated nanoholes shows negligible variation, effectively 'masking'

the theoretical optical elongation.

3. Sensing mechanism

Rhodamine 6G (Rh6G) tends to form aggregates at higher concentration, leading to the formation of dimers and higher aggregate structures. The solvent system also plays a role in aggregation because of the hydrophobic alkyl groups on the Rh6G molecule. Polar protic solvents (ethanol) promote aggregation while polar aprotic solvents (acetone) hinder the aggregation process, and nonpolar solvents (e.g., toluene) can induce de-aggregation.

The inner surface of nanostructured sapphire crystal (SC) is predominantly covered with surface hydroxyl groups (aluminol, –Al–OH) and surface defect sites, such as Lewis acidic unsaturated Al^{3+} and O^{2-} centers[1]. When Rh6G molecules are introduced into the nanopores, they interact with these surface functionalities. Under ambient conditions, the aluminol groups serve as the primary adsorption sites, facilitating dye immobilization through hydrogen bonding or electrostatic interactions, whereas defect sites may contribute more significantly under dehydrated conditions. Consequently, Rh6G molecules are immobilized on the pore walls in monomeric or dimeric forms, governed by a surface chemistry that is effectively dominated by aluminol group functionalities.

Figure S10 illustrates the nanohole surface where dimers are adsorbed. While it is well-known that inner walls of the nanohole**s** is naturally irregular rather than ideally flat, the irregularities can be considered minimized at small length scales[3]. Furthermore, since the nanopores in SC are unidirectionally connected, the deviation from a flat plane at the molecular adsorption scale is not significant.

The mobility of Rh6G molecules in the dried SC matrix is limited, preventing multiple monomers from diffusing to form large aggregates. Moreover, the hydrophilic character of the SC surface favors Rh6G molecular adsorption in a perpendicular rather than a parallel arrangement relative to the surface.

Incorporation of Rh6G into a solid host matrix significantly alters its photophysical properties. As a result, Rh6G immobilized in SC exhibits pronounced differences in absorption and fluorescence behaviors compared with those observed in solution [4]. These characteristics make Rh6G-SC a promising sensor to alcohol gas.

3.Supplementary figures

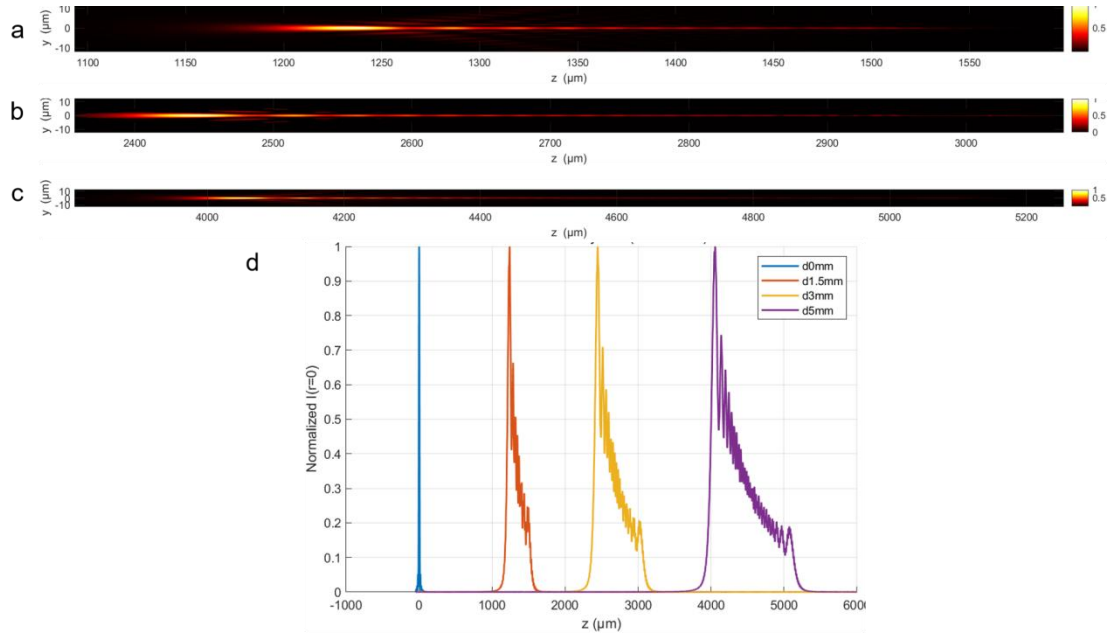

Fig. S1. Numerical simulations of the focal-intensity distribution under spherical-aberration-enhanced focusing for YAG cover-plate thicknesses of (a) 1 mm, (b) 3 mm, and (c) 5 mm. Increasing the YAG thickness introduces stronger refractive-index–mismatch–induced spherical aberration, leading to a progressive axial elongation of the focal region. (d) On-axis normalized intensity profiles comparing focusing without a cover plate and with 1 mm, 3 mm, and 5 mm YAG cover plates, highlighting the substantial extension of the focal depth.

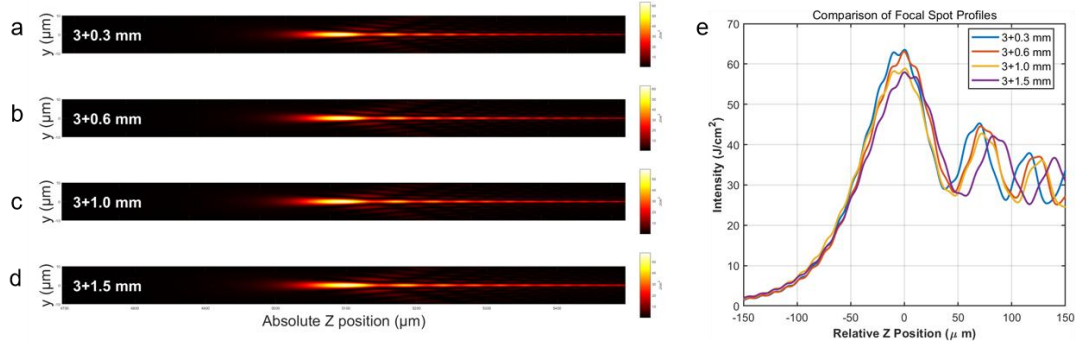

Fig. S2. Numerical simulations of focal intensity distributions at varying fabrication depths. (a–d) optical intensity distributions simulated at depths of (a) 0.3 mm, (b) 0.6 mm, (c) 1.0 mm, and (d) 1.5 mm within the sapphire substrate. (e) Comparison of the corresponding on-axis intensity profiles. The simulation incorporates a fixed 3-mm-thick YAG cover plate to induce strong spherical aberration. As the focus moves deeper into the substrate, the focal line exhibits a moderate and gradual axial elongation due to the accumulation of spherical aberration. However, the elongated "needle-like" filament morphology is robustly preserved across all depths. This stability ensures consistent high-aspect-ratio modification capability, supporting the uniformity of the stitched waveguide structures.

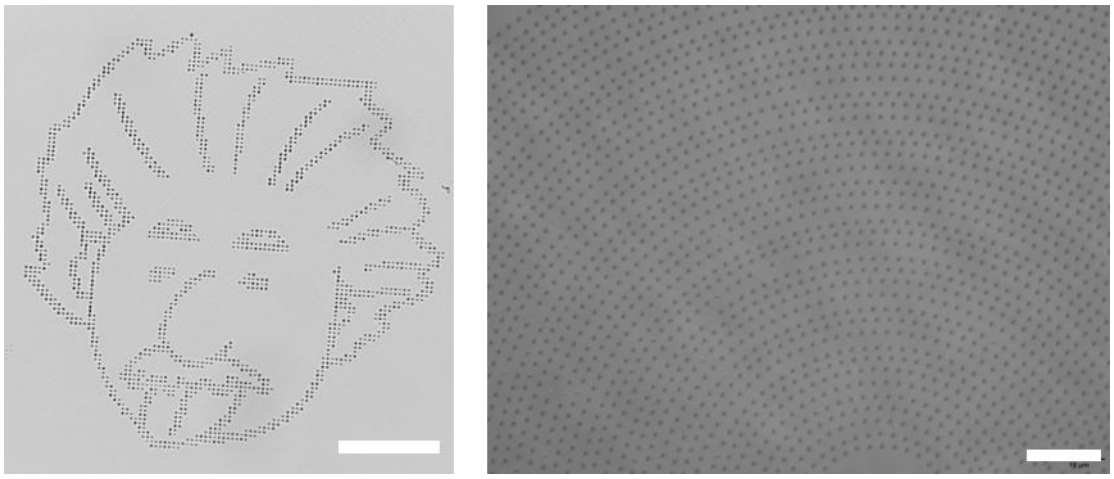

Fig. S3. The large-area patterned structures fabricated by wet-etching-assisted single-pulse nanolithography (WESPN) (Scale bar: 100 μm、60μm).

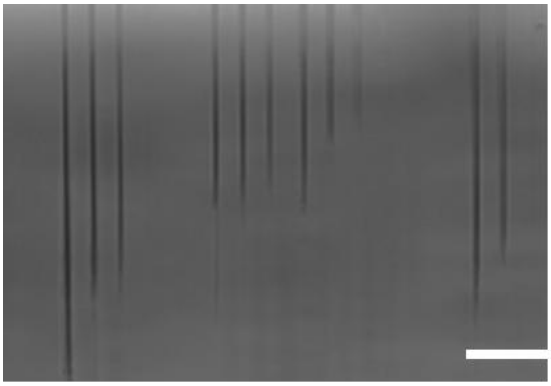

Fig. S4. The variation in nanohole length with respect to different pulse energies and number of pulses. (Scale bar: 50μm)

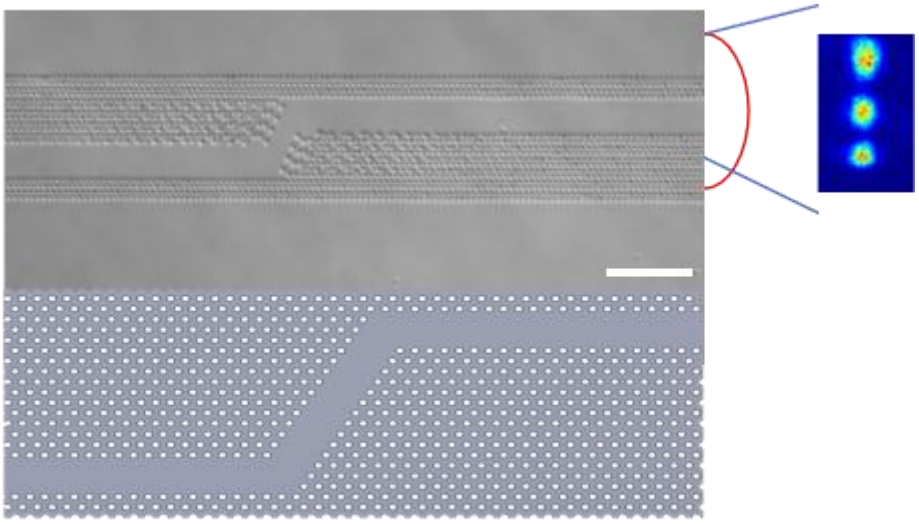

Fig. S5. Microscope images, schematic diagrams, and mode field profiles of Z-shaped waveguides. (Scale bar: 15μm)

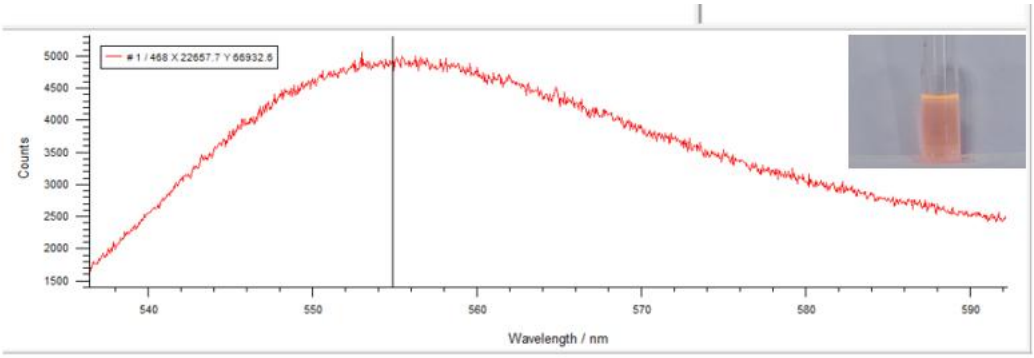

Fig. S6. Intensity versus wavelength plots for photonic crystal waveguide-based ethanol detection, and Rhodamine-alcohol solution spectra.

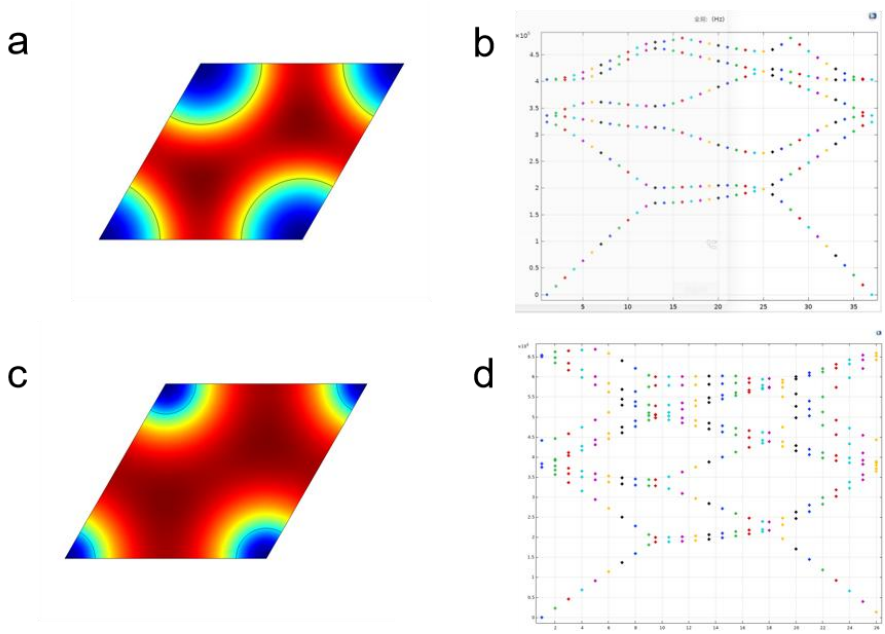

Figure S7. (a) Simulated focal-intensity distribution for a nanohole array with a hole diameter of 300 nm. (b) Corresponding simulated photonic bandgap for the structure with 300 nm holes. (c) Simulated focal-intensity distribution for a nanohole array with a hole diameter of 150 nm. (d) Corresponding simulated photonic bandgap for the structure with 150 nm holes. The simulations demonstrate that although both structures exhibit periodicity, the resulting bandgap is not comparable to that of a traditional photonic crystal waveguide. Instead, the structures function as nanohole-clad waveguides, with the light confined within the sapphire core.

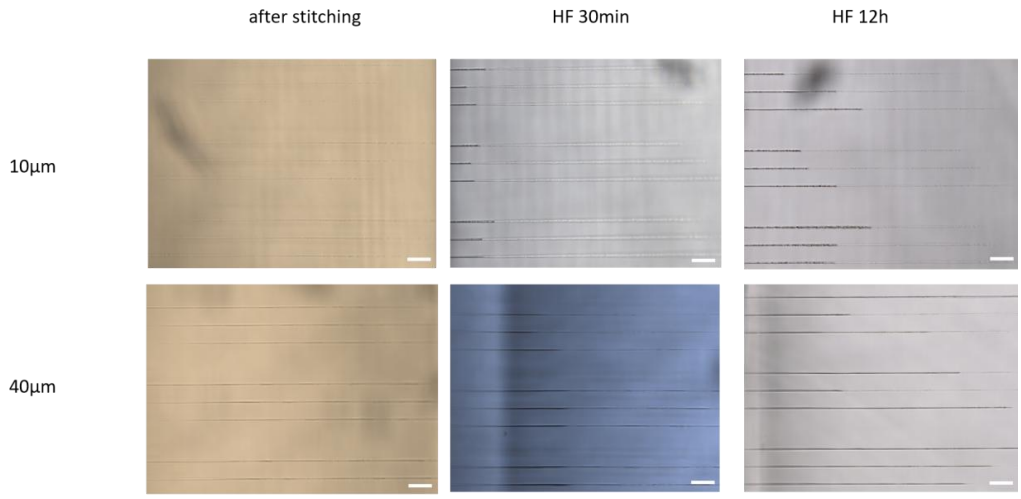

Fig. S8. To investigate the influence of axial stitching distance on the structural quality of the nanoholes, we varied the single-step displacement within the same sample. The results show that when the stitching distance is too short, excessive overlap between successive laser pulses leads to roughened sidewalls and incomplete etching, with a significantly reduced etching rate. In contrast, when the stitching distance is approximately equal to the single-pulse modification depth, smooth and continuous nanoholes are obtained, and the etching proceeds uniformly through the entire structure." (Scale bar: 25μm)

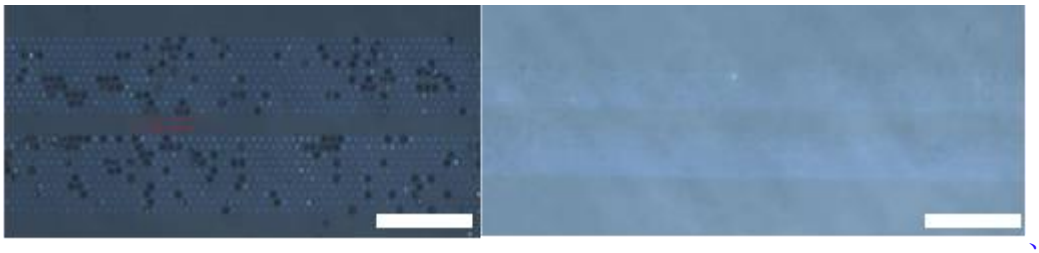

Figure S9. Optical microscopy top-view of the Deep-Nanohole-Clad waveguide fabricated in quartz glass and YAG. The overall waveguide structure and the periodic pattern of the cladding region are clearly visible. (Scale bar: 15μm、25μm)

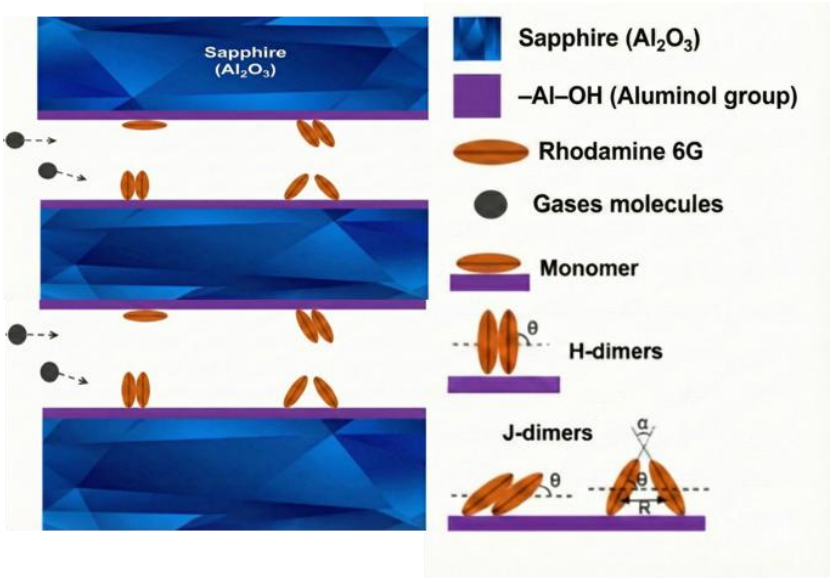

Figure S10. Schematic representation of Rh6G molecules immobilized in the inner wall of nanopores of SC. [3]

References

1. Eaton, S.M., Zhang, H.B. & Herman, P.R. Heat accumulation effects in femtosecond laser-written waveguides with variable repetition rate. *Optics Express* **13**, 4708-4716 (2005).
2. Huang, L. et al. Aberration correction for direct laser written waveguides in a transverse geometry. *Optics Express* **24** (2016).
3. del Monte, F. & Levy, D. Identification of oblique and coplanar inclined fluorescent J-dimers in rhodamine 110 doped sol-gel-glasses. *The Journal of Physical Chemistry B* **103**, 8080-8086 (1999).
4. Del Monte, F., Mackenzie, J.D. & Levy, D. Rhodamine fluorescent dimers adsorbed on the porous surface of silica gels. *Langmuir* **16**, 7377-7382 (2000).